Application and properties of the radon transform for object image matching

Conference Paper · January 2017
DOI: 10.1109/SAMI.2017.7880333

3 authors:

Gábor Kertész
Óbudai Egyetem
12 PUBLICATIONS **20** CITATIONS
SEE PROFILE

Sandor Szenasi
Óbudai Egyetem
59 PUBLICATIONS **179** CITATIONS
SEE PROFILE

Zoltan Vamossy
Óbudai Egyetem
120 PUBLICATIONS **291** CITATIONS
SEE PROFILE

Application and properties of the Radon transform for object image matching

Gábor Kertész, Sándor Szénási, Zoltán Vámossy
John von Neumann Faculty of Informatics
Óbuda University
{kertesz.gabor, szenasi.sandor, vamossy.zoltan}@nik.uni-obuda.hu

***Abstract*—The Radon transform and the reverse formulas are mostly used in computer tomography to reconstruct the original shape. The projections of an image could be used in computer vision for object recognition, based on projection matching. By comparing the projections, an effective method could be defined. To understand the projection behavior the basic properties of the transform are inspected, and the results of several image transformations are analyzed.**

I. Introduction

The Radon transform is a mapping that processes two-dimensional data, and results in its one-dimensional projections. The formula and its inverse are widely used.

The original mapping was first studied by Johann Radon [1] in 1917, a translation of his paper was published in 1986 [2]. The formula and the inversion formula is used with the CT, PET or MR scanners to create images from the obtained data. Other application fields include electron microscopy [3], astronomy, and geophysics [4].

The projections of an image could be used in computer vision for object recognition [5]: by calculating projections for various rotational angles, the achieved image signature could be used to compare images.

In [6], the horizontal and vertical projections of the image are extended with the diagonal and antidiagonal projections to complete a so-called image signature, and based on these signatures effective object matching can be achieved [5] (as seen on Fig. 1).

II. Theory

The Radon transform is usually defined as

$$\check{f} = \mathcal{R}f = \int_L f(x,y)\mathrm{d}s, \tag{1}$$

where x, y are coordinates of points on the plane, and f is a function defined on $\mathbb{R}^2$. The projection or line integral is based on line $L \in \mathbb{R}^2$, and $\mathrm{d}s$ is an increment along L [4]. Notable, that there are multiple generalized forms of the transform, where the domain is extended to higher dimensions (such as $\mathbb{R}^2$ or $\mathbb{R}^n$).

A line could be given in normal form as

$$p = xcos(\phi) + ysin(\phi), \tag{2}$$

where ϕ is the angle of rotation. From p and ϕ we can give the Radon transform of $f(x, y)$ as

$$\check{f}(p,\phi) = \mathcal{R}f = \int_L f(x,y)\mathrm{d}s. \tag{3}$$

A rotated coordinate system with axes p and s could be presented by applying the rotation matrix $Rot(\phi)$ as

$$\begin{aligned}\begin{bmatrix} p \\ s \end{bmatrix} &= Rot(\phi) \times \begin{bmatrix} x \\ y \end{bmatrix} \\ &= \begin{bmatrix} \cos\phi & -\sin\phi \\ \sin\phi & \cos\phi \end{bmatrix} \begin{bmatrix} x \\ y \end{bmatrix} \\ &= \begin{bmatrix} x\cos(\phi) + y\sin(\phi) \\ y\cos(\phi) - x\sin(\phi) \end{bmatrix}.\end{aligned} \tag{4}$$

Having axes p and s of the new coordinate system, then

$$\begin{aligned} x &= p\cos(\phi) - s\sin(\phi) \\ y &= p\sin(\phi) + s\cos(\phi), \end{aligned} \tag{5}$$

resulting with the form of the Radon transform in

$$\check{f}(p,\phi) = \int_{-\infty}^{\infty} f(p\cos(\phi) - s\sin(\phi), p\sin(\phi) + s\cos(\phi))\mathrm{d}s. \tag{6}$$

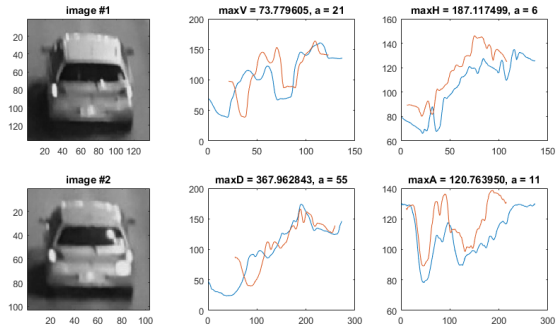

Fig. 1. The projection profiles could be used to compare and match detected objects [5]. The vehicles on image #1 and image #2 are the same, but the images are from different frames of a video stream, even the sizes are different. The charts on the top row show the vertical and horizontal projections, while the bottom row presents the diagonal and antidiagonal projection profiles, respectively.

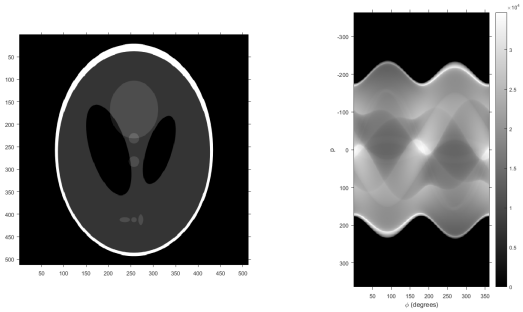

Fig. 2. The Shepp-Logan [7] phantom is a standard test image used in the testing of image reconstruction algorithms: it consists of 10 different sized, rotated ellipses with different intensity levels in a squared area.

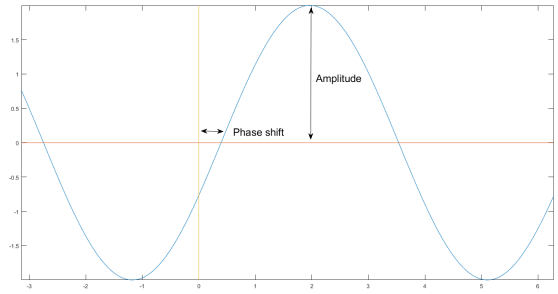

Fig. 3. The transformation of the sinus wave is formalized as $A\sin(\alpha+\beta)$, where A stands for the amplitude and β is the phase shift.

III. Properties

The visual representation of the Radon transform is often referred as a sinogram, where p projection sums are presented for each ϕ angle. A sample of a the sinogram representation is on Fig. 2.

The name sinogram is based on the sinusoid representation of the points. The reason of the sinus wave could be simply proven: the representation of point $P(x_0, y_0)$ in the Radon space can be given as

$$p = x_0\cos(\phi) + y_0\sin(\phi), \tag{7}$$

which can be reducted to a sinus function using

$$sin(\alpha + \arctan(z)) = \frac{z\cos(\alpha) + \sin(\alpha)}{\sqrt{1+z^2}} \tag{8}$$

as

$$\frac{p}{y_0} = \frac{x_0}{y_0}\cos(\phi) + \sin(\phi) \tag{9a}$$

$$\frac{\frac{p}{y_0}}{\sqrt{1+\left(\frac{x_0}{y_0}\right)^2}} = \frac{\frac{x_0}{y_0}\cos(\phi) + \sin(\phi)}{\sqrt{1+\left(\frac{x_0}{y_0}\right)^2}} \tag{9b}$$

$$\frac{\frac{p}{y_0}}{\sqrt{1+\left(\frac{x_0}{y_0}\right)^2}} = sin(\phi + \arctan(\frac{x_0}{y_0})) \tag{9c}$$

$$\frac{p}{y_0\sqrt{1+\left(\frac{x_0}{y_0}\right)^2}} = sin(\phi + \arctan(\frac{x_0}{y_0})) \tag{9d}$$

$$p = y_0\sqrt{1+\left(\frac{x_0}{y_0}\right)^2}\, sin(\phi + \arctan(\frac{x_0}{y_0})) \tag{9e}$$

$$p = \sqrt{x_0^2+y_0^2}\, sin(\phi + \arctan(\frac{x_0}{y_0})). \tag{9f}$$

Equation 9f basically defines a sinus wave [8] with amplitude

$$A = \sqrt{x_0^2+y_0^2} \tag{10}$$

and phase shift

$$\theta = \arctan(\frac{x_0}{y_0}), \tag{11}$$

visible on Fig. 3.

IV. Image projection properties

When using the Radon transform on a 2D image, some properties of the form can be generalized, or simplified. First of all, having image as an $N \times N$ matrix I, the integrals calculated for each line are basically the sums of the affected pixel intensities.

Please note, that the this paper concentrates on the properties and specialties of the Radon transform of squared images.

The size of the result matrix needs to be defined according to the longest projection of the image, which is the diagonal. For a squared, $N \times N$ image it is given by $\sqrt{2}N$.

The sampling rate of ϕ is a key factor: increasing the step size causes less computation, however larger step sizes result in projection data loss. The range of the value of ϕ is $[0, 2\pi]$. However, it is notable, that the range of $(\pi; 2\pi)$ is the same as the values in $(0; \pi)$, only mirrored around p axis.

Because of the mirroring effect, it is only necessary to define the projection sums p of I image in the range $[0, \pi]$ of ϕ. The optimal step-size depends on multiple assumptions, mostly on matrix size N, so in this paper we will refer to it as $Step(N)$.

A. Key points

Since the sinogram size is defined as an R_f matrix $\sqrt{2}N \times \frac{\pi}{Step(N)}$, and the input is an $N \times N$ matrix referred as I, a few specialties could noticed.

The first interesting property of the application of the Radon transform on squared input is, that R_f result matrix will have

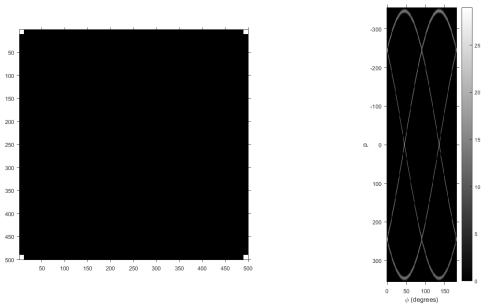

Fig. 4. On the left hand side is the image representation of the matrix defined in Eq. 12. On the right hand side is the sinogram of the Radon transform of the image. Note, that the regions above and below the projection of the corner points are insignificant.

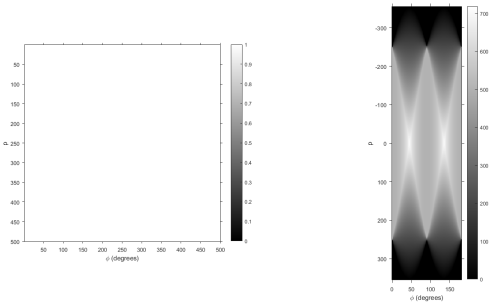

Fig. 5. On the left hand side is the image representation of the unit matrix defined in Eq. 13. On the right hand side is the sinogram of the Radon transform of this image. Note, that the intensity is affected by the number of pixels summarized: the brightest points are in the centers of the diagonal and antidiagonal projections at $\pi/4$ and $3\pi/4$.

regions, where the sum is always zero, because the lack of crossing pixels.

In Fig. 4 the sample matrix is defined with zero values, whereas the corner points have unit intensities as

$$I_1 = \begin{bmatrix} 1 & 0 & 0 & 0 & ... & 1 \\ 0 & 0 & 0 & 0 & ... & 0 \\ 0 & 0 & 0 & 0 & ... & 0 \\ 0 & 0 & 0 & 0 & ... & 0 \\ ... & & & & & \\ 1 & 0 & 0 & 0 & ... & 1 \end{bmatrix}. \tag{12}$$

As visible, the regions over and below these boundaries are insignificant. As in Fig. 5, where the input matrix is a unit matrix, where all values are equal to one, as

$$I_2 = \begin{bmatrix} 1 & 1 & 1 & 1 & ... & 1 \\ 1 & 1 & 1 & 1 & ... & 1 \\ 1 & 1 & 1 & 1 & ... & 1 \\ 1 & 1 & 1 & 1 & ... & 1 \\ ... & & & & & \\ 1 & 1 & 1 & 1 & ... & 1 \end{bmatrix}, \tag{13}$$

the same effect can be noticed.

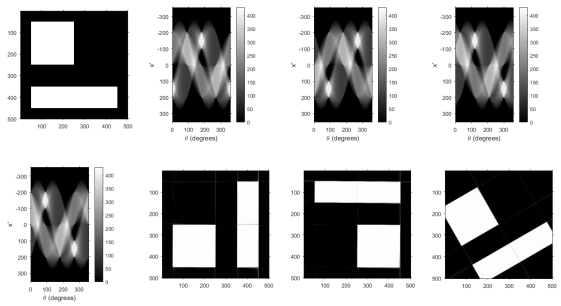

Fig. 6. The original image on the top-left, and the sinogram of its projection sums are presented on the bottom-left. To illustrate the effect of the circular shifting, the resulting matrix is shifted by ϕ. The top row shows sinograms after shifting with $\pi/2$, π and $\pi/6$, respectively. The bottom row shows the result of the reconstruction after shifting.

B. Rotation, mirroring

The most trivial property of the Radon transform is, that the rotation of input image $I = f(x, y)$ effects on $\check{f}(p, \phi)$ sinogram as a linear shifting. As a result, the rotation of the object of interest does not affect the projection based recognition, since it leads to a circular shift in the projection space.

On Fig. 6 the circular shifting phenomena is proved by applying the Radon inversion formula. The inversion formula is used to reconstruct the original image from its projections. The basic formula is given in the original work of Radon [1] [2], however there are multiple approaches for reconstruction, based on the Fourier slice theorem [9], or on filtered backprojection [10].

While the α angled rotation of the image results in an $\frac{\alpha}{Step(N)}$ circular shift on R_f sinogram, if the object is mirrored, the resulting sinogram is rotated by 180 degrees, which is the same as considering the reflection from left to right, and then upside-down.

C. Shift

The horizontal or vertical translation of an object by $\Delta x, \Delta y$ on input I could be denoted as

$$p_s(\phi) = \Delta x \cos(\phi) + \Delta y \sin(\phi). \tag{14}$$

Using Eq. 1, this results in

$$\mathcal{R}f = \check{f}(p - p_s(\phi), \phi). \tag{15}$$

As visualized on Fig. 7, the horizontal translation of the object results in amplitude and phase changes in the sinusoids. The differences are highlighted on Fig. 8.

Vertical translation or scaling have the same effects on the sinogram.

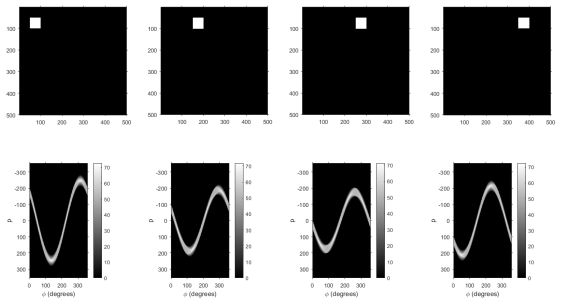

Fig. 7. The results of horizontal translation on the sinogram: the front row shows the input image, where the object is shifted to the right, and the bottom row presents the sinograms for each input image.

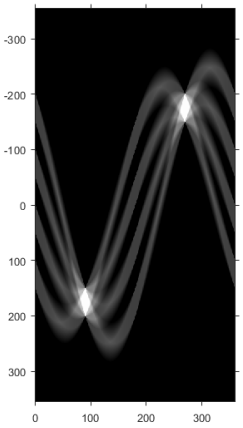

Fig. 8. The highlighted results of the comparison on 7. The horizontal shifting affects the amplitude and phase of the sinusoid.

D. Intensity

Another trivial property of the Radon transform is, that if the intensity of the visual representation of the object changes, it affects the projection sums, however the form of the wave is unaffected. On Fig. 9 this phenomena is visualized by all sinogram presenting the very same form. Please note, that the intensity levels of each sinogram differ. In this special case, the normalization of the sinograms results in equivalent matrices.

E. Noise

In computer vision and image processing, noise removal is an important procedure, with multiple different approaches [11]. The effects of noise on the projections sums of an image are very significant (Fig. 10 a, b).

There are multiple filters, which could be applied to reduce the noise on a 2D image. However recent studies [12] show, instead of denoising the input image (as seen on 10 c), noise reduction filters could be used in the Radon space.

Please note, that the filtered backprojection itself comes with minor data loss: by using the inverse radon formula, the reconstructed image will lose some data - and noise (Fig. 10 d).

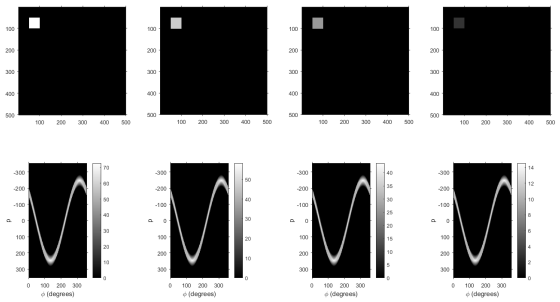

Fig. 9. The effect of intensity changes on the sinogram. The front row shows the input image, where the object intensity is 1, 0.8, 0.6 and 0.2, respectively, and the bottom row presents the sinograms for the input images.
Please note, that while the form of the sinusoids are the same, the intensity levels (visible on the bars) are different.

To illustrate the effects of applying filtering in the Radon space, Fig. 10 e shows the denoised sinogram, where each projection function was denoised using a simple moving average filter. After denoising of each projections, the reconstructed image is represented on Fig 10 f.

V. Suggestion

As seen above, it is understandable, that the result of Radon transform - when applied to an image - could be used for object matching. While it is highly sensitive to noise, noise reduction filters could be applied in Radon space.

However, few disadvantages of the method are visible: the blank areas on the sinogram could hold up memory space in a possible implementation. To resolve this issue, the size of the result matrix should be fixed, and the input values should be standardized, using fixed scales [13]. This can be achieved by using a simple procedure, rotating a projection segment around the image, and by dividing this segment to fixed number of subsegments (Fig. 11).

Another issue that needs resolution is the phenomena that happens when lowering the intensity values: the form of the sinogram is the same, however the spectrum differs. A simple solution is to normalize the result matrix.

To introduce the differences between the Radon transform, and this method based on simple trigonometric functions (Fig. 12 and Fig. 13), it is clear, that the form of the sinogram kept, but stretched to a fixed height.

Although the method clearly changed from the original Radon transform, the memory handling is more reasonable (Table I). Test results also indicate, that the multi-parallel solution implemented on a GPU have remarkable performance [13].

VI. Summary

This paper showed the method and basics of the Radon transform, from the original idea, to its applications and properties.

The so-called sinogram representation is analyzed, and the effects of some image transformations are studied.

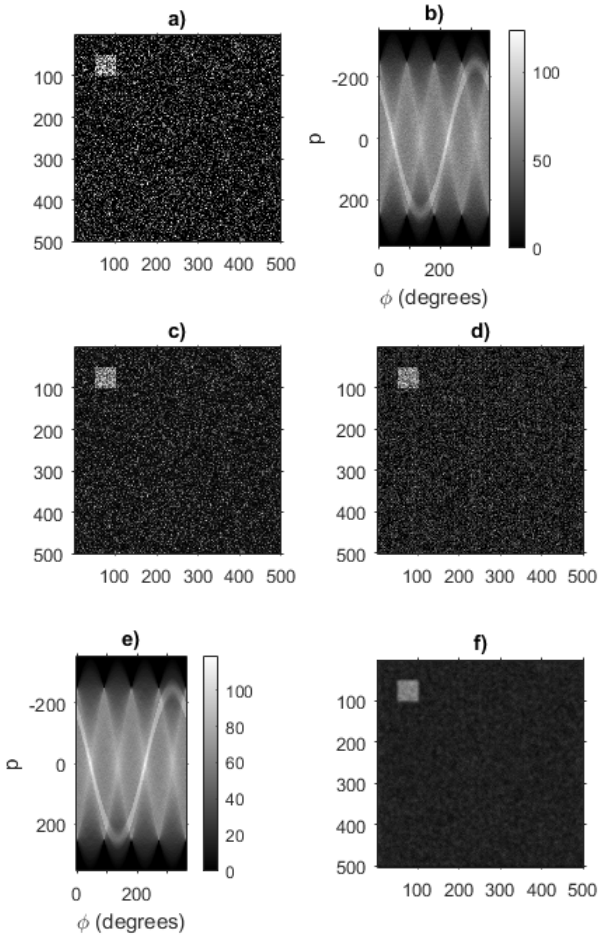

Fig. 10. a) Original image with a zero mean, 0.1 variance Gaussian noise b) The sinogram of the original image c) The Gauss filtered original image d) The reconstructed image e) The sinogram after mean filtering each column f) The reconstructed image of e)

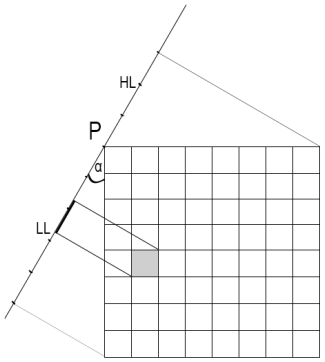

Fig. 11. The proposal in [13] is based on trigonometrical functions: with the rotation of a line placed on the left side of the image, the top and bottom length of the projection (HL, LL) can be calculated, and the segment provided by $HL + LL$ is divided into N different parts, where N is the width and height of the squared image.

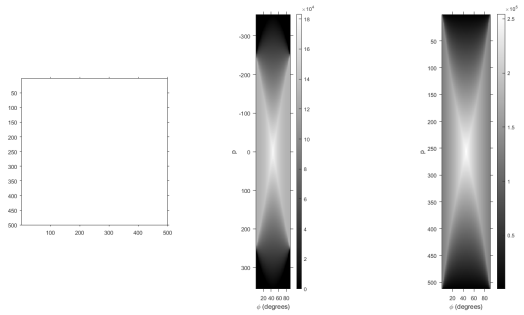

Fig. 12. The original image of a unit matrix, the Radon transform of the unit matrix from 0 degrees to 90 degrees, and the result of the method proposed in [13], respectively.

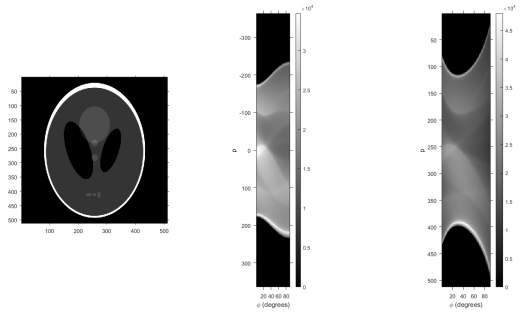

Fig. 13. The original image of the Shepp-Logan phantom, the Radon transform of the phantom starting from 0 degrees to 90 degrees, and the result of the method proposed in [13], respectively.

It is understandable, that the projection profile of an image could be used for object matching: however, a refined method should be used instead of the Radon transform. The methodology suggested in [13] is applied to visualize the differences of the two methods.

Our further plans include the further research, and GPU-based implementation of the proposed method. The provided results show, that projection-based object matching could be used in certain applications [6] [14] [15] [16].

Further research includes the comparison of noise removal

TABLE I
MEMORY ALLOCATION OF EACH METHOD, FOR 90 MEASUREMENTS (FROM 0 DEGREE TO 90 DEGREES OF ROTATION)

Image size (pixels)	**Result size of the Radon transform**	**Result size in the presented method**
160	20657	14560
320	41223	29120
480	61789	43680
640	82446	58240
800	103012	72800
960	123578	87360
1120	144144	101920
1280	164801	116480
1440	185367	131040
1600	205933	145600

filters, which could be applied in the projection space, and analysis of the result of different projection matching methods.

A. Acknowledgements

The authors would like to thank the members of the GPU Education Center (formerly known CUDA Teaching Center) at Óbuda University for their constructive comments and suggestions.

The authors acknowledge the support of the Doctoral School of Applied Informatics and Applied Mathematics of Óbuda University.

The authors would also like to say thanks for the help of the Hungarian National Talent Program (NTP-SZKOLL-16).

REFERENCES

[1] J. Radon, "Über die Bestimmung von Funktionen durch ihre Integralwerte längs gewisser Mannigfaltigkeiten," *Berichte über die Verhandlungen der Königlich-Sächsischen Akademie der Wissenschaften zu Leipzig, Mathematisch-Physische Klasse*, pp. 262–277, 1917.

[2] ——, "On the determination of functions from their integral values along certain manifolds," *Medical Imaging, IEEE Transactions on*, vol. 5, pp. 170–176, 1986.

[3] P. J. Drew, P. Blinder, G. Cauwenberghs, A. Y. Shih, and D. Kleinfeld, "Rapid Determination of Particle Velocity from Space-time Images Using the Radon Transform," *J. Comput. Neurosci.*, vol. 29, no. 1-2, pp. 5–11, Aug. 2010. [Online]. Available: http://dx.doi.org/10.1007/s10827-009-0159-1

[4] S. R. Deans, *The Radon Transform and Some of Its Applications*, 1983.

[5] G. Kertész, S. Sergyán, S. Szénási, and Z. Vámossy, "Implementation of Object Recognition based on Image Projection Signatures using Matlab," *CINTI 2016 - 17th IEEE International Symposium on Computational Intelligence and Informatics*, 2016.

[6] V. Jelača, A. Pižurica, J. O. Niño-Castañeda, A. Frías-Velázquez, and W. Philips, "Vehicle matching in smart camera networks using image projection profiles at multiple instances," *Image and Vision Computing*, vol. 31, pp. 673–685, 2013.

[7] L. A. Shepp and B. F. Logan, "The Fourier reconstruction of a head section," *IEEE Transactions on Nuclear Science*, vol. 21, pp. 21–43, 1974.

[8] G. R. Gindi and A. F. Gmitro, "Optical feature extraction via the Radon transform," *Optical Engineering*, vol. 23, pp. 499–506, 1984.

[9] I. Y. Chun, B. Adcock, and T. M. Talavage, "Non-convex compressed sensing CT reconstruction based on tensor discrete Fourier slice theorem," *Engineering in Medicine and Biology Society (EMBC), 2014 36th Annual International Conference of the IEEE*, 2014.

[10] R. Clackdoyle, F. Noo, and M. S. O. Mohamed, "Filtered-Backprojection Reconstruction Formula for 2D Tomography with Bilateral Truncation," *Nuclear Science Symposium Conference Record, 2006. IEEE*, 2006.

[11] R. Szeliski, *Computer Vision: Algorithms and Applications*, 1st ed. New York, NY, USA: Springer-Verlag New York, Inc., 2010.

[12] X. Zhu, X. Yang, Q. Zhou, L. Wang, F. Yuan, and Z. Bian, "A Wavelet Multiscale De-Noising Algorithm Based on Radon Transform," *Wavelet Transforms and Their Recent Applications in Biology and Geoscience*, 2012.

[13] G. Kertész, S. Szénási, and Z. Vámossy, "A Novel Method for Robust Multi-Directional Image Projection Computation," *INES 2016 - 20th IEEE International Conference on Intelligent Engineering Systems*, 2016.

[14] D. Stojcsics, L. Somlyai, and A. Molnár, "Unmanned aerial vehicle guidance methods for 3D aerial image reconstruction," *ICCC 2013, Proceedings of IEEE 9th International Conference on Computational Cybernetics*, pp. 321–326, 2013.

[15] A. Molnár, D. Stojcsics, and I. Lovas, "Precision agricultural and game damage analysis application for unmanned aerial vehicles," *INTERNATIONAL JOURNAL OF APPLIED MATHEMATICS AND INFORMATICS*, vol. 10, pp. 38–43, 2016.

[16] Á. Takács, D. Á. Nagy, I. J. Rudas, and T. Haidegger, "Origins of Surgical Robotics: From Space to the Operating Room," *Acta Polytechnica Hungarica*, vol. 13, pp. 13–30, 2016.